Converging structural and functional connectivity of orbitofrontal, dorsolateral prefrontal, and posterior parietal cortex in the human striatum

Kevin Jarbo & Timothy D. Verstynen

Department of Psychology,
Center for the Neural Basis of Cognition
Carnegie Mellon University
Pittsburgh, PA 15213

Abbreviated Title: Converging connectivity in the human striatum

Corresponding Author:
Kevin Jarbo
Carnegie Mellon University
Department of Psychology
Baker Hall 342C
Pittsburgh, PA 15213
kjarbo@andrew.cmu.edu
(412) 268-7136 (office phone)

Pages: 36 (w/o references), 42 (w/references)
Figures: 7
Tables: 1
Multimedia and 3D Models: 0
Words: Abstract (239), Introduction (443), Discussion (1530)

Conflict of Interest: The authors do not have any conflicts of interest to report.

Acknowledgements:
The authors would like to thank Dr. Roberta Klatzky for her consultation regarding data analyses used in this document. This research was sponsored by the PA Department of Health Formula Award #SAP4100062201 and by the Army Research Laboratory under Cooperative Agreement Number W911NF-10-2-0022. The views and conclusions contained in this document are those of the authors and should not be interpreted as representing the official policies, either expressed or implied, of the Army Research Laboratory or the U.S. Government. The U.S. Government is authorized to reproduce and distribute reprints for Government purposes notwithstanding any copyright notation herein.

Abstract

Modification of spatial attention via reinforcement learning (Lee & Shomstein, 2013) requires the integration of reward, attention, and executive processes. Corticostriatal pathways are an ideal neural substrate for this integration because these projections exhibit a globally parallel (Alexander, DeLong, & Strick, 1986), but locally overlapping (Haber, 2003), topographical organization. Here we explore whether there are unique striatal regions that exhibit convergent anatomical connections from orbitofrontal cortex (OFC), dorsolateral prefrontal cortex (DLPFC), and posterior parietal cortex. Deterministic fiber tractography on diffusion spectrum imaging data from neurologically healthy adults (N=60) was used to map fronto- and parieto-striatal projections. In general, projections from cortex were organized according to both a medial-lateral and a rostral-caudal gradient along the striatal nuclei. Within rostral aspects of the striatum we identified two bilateral convergence zones—one in the caudate nucleus and another in the putamen—that consisted of voxels with unique projections from OFC, DLPFC, and parietal regions. The distributed cortical connectivity of these striatal convergence zones was confirmed with follow-up functional connectivity analysis from resting state fMRI data, in which a high percentage of structurally connected voxels also showed significant functional connectivity. The specificity of this convergent architecture to these regions of the rostral striatum was validated against control analysis of connectivity within the motor putamen. These results delineate a neurologically plausible network of converging corticostriatal projections that may support the integration of reward, executive control, and spatial attention that occurs during spatial reinforcement learning.

Introduction

It is well known that contextual factors, like cue/target proximity within the same bounded object, can bias bottom-up visuospatial attention (Egeth & Yantis, 1997; Posner, Snyder, & Davidson, 1980). Recent research has shown that placing a high reward on certain targets can override this intrinsic spatial attention bias (Della Libera & Chelazzi, 2006; Kristjansson, Sigurjonsdottir, & Driver, 2010; Lee & Shomstein, 2013b, 2014). The abrogating influence of reward feedback on intrinsic spatial attention is consistent with the idea that reinforcement learning (Sutton & Barto, 1998) alters the bottom-up influences of stimulus features on attentional allocation during spatial decision making.

Functionally, reinforcement learning depends on the striatum (Daw & Doya, 2006; Dayan & Abbott, 2001; Graybiel, 1995; Knutson, Westdorp, Kaiser, & Hommer, 2000; O'Doherty, 2004). While many studies focus on the role of the ventral striatum in reinforcement learning (Mcclure, York, & Montague, 2004; O'Doherty, Dayan, Friston, Critchley, & Dolan, 2003; Pagnoni, Zink, Montague, & Berns, 2002; Rodriguez, Aron, & Poldrack, 2006), evidence of dorsomedial caudate involvement in reward-based responses suggests a more global involvement of striatal systems in behavioral updating (Delgado, Locke, Stenger, & Fiez, 2003; Delgado, Miller, Inati, & Phelps, 2005; Knutson & Cooper, 2005; Kuhnen & Knutson, 2005; Lohrenz, McCabe, Camerer, & Montague, 2007). This recruitment of distributed striatal systems may reflect an integration of multiple, disparate signals during learning. Indeed, while the striatum is generally viewed as a central integration point of cortical information within strictly closed, but parallel circuits (Alexander et al., 1986), there is a growing body of evidence for overlap from spatially disparate cortical areas (Averbeck, Lehman, Jacobson, & Haber, 2014; Haber, 2003). This diffuse overlap of corticostriatal projections has been proposed as an explicit

substrate for reinforcement learning that directly integrates reward and executive control signals from the orbitofrontal (OFC) and dorsolateral prefrontal cortex (DLPFC), respectively (see Haber & Knutson, 2010 for review).

Introducing signals from regions that support visuospatial processing into this striatal integration process may be one mechanism by which reinforcement learning can be applied to spatial attention. Visuospatial attention is generally associated with the posterior parietal cortex in humans and nonhuman primates (see Colby & Goldberg, 1999; Critchely, 1953; Silver, Ress, & Heeger, 2005 for review). Nonhuman primate histology research has a shown a topography of parietostriatal connectivity in which posterior parietal projections terminate is distributed clusters along the caudate nucleus, proximal to OFC and DLFPC projection termination sites (Cavada & Goldman-Rakic, 1991; Selemon & Goldman-Rakic, 1985, 1988). This proximity of DLPFC and parietal connectivity has also recently been confirmed functionally in humans (Choi, Yeo, & Buckner, 2012; Di Martino et al., 2008); however, the specific pattern of convergent inputs from parietal, DLPFC and OFC areas has yet to be confirmed.

To this end, we used diffusion spectrum imaging (DSI) and resting state fMRI to explore a neurologically plausible network of converging projections in the striatum that may support the integration of information from OFC, DLPFC, and posterior parietal areas. The presence of convergent corticostriatal inputs would provide necessary evidence for a structurally and functionally integrative network that underlies mechanisms of spatial reinforcement learning.

Materials and Methods

Participants

Sixty participants (28 male, 32 female) were recruited locally from the Pittsburgh, Pennsylvania area as well as the Army Research Laboratory in Aberdeen, Maryland. Participants were neurologically healthy adults with no history of head trauma, neurological or psychological pathology. Participant ages ranged from 18 to 45 years old (mean age 26.5 years old). Informed consent, approved by the Institutional Review Board at Carnegie Mellon University and in compliance with the Declaration of Helsinki, was obtained for all participants. Participants were all financially compensated for their time.

MRI Acquisition

All 60 participants were scanned at the Scientific Imaging and Brain Research (SIBR) Center at Carnegie Mellon University on a Siemens Verio 3T magnet fitted with a 32-channel head coil. A magnetization prepared rapid gradient echo imaging (MPRAGE) sequence was used to acquire a high-resolution (1mm^3 isotropic voxels, 176 slices) T1-weighted brain image for all participants. DSI data was acquired following fMRI sequences using a 50-minute, 257-direction, twice-refocused spin-echo EPI sequence with multiple q values (TR = 11,400ms, TE = 128ms, voxel size = 2.4mm^3, field of view = 231 x 231mm, b-max = 5,000s/mm^2, 51 slices). Resting state fMRI (rsfMRI) data consisting of 210 T2*-weighted volumes were collected for each participant with a blood oxygenation level dependent (BOLD) contrast with echo planar imaging (EPI) sequence (TR = 2000ms, TE = 29ms, voxel size = 3.5mm^3, field of view = 224 x 224mm, flip angle = 79°). Head motion was minimized during image acquisition with a custom foam padding setup designed to minimize the variance of head motion along the pitch and yaw rotation directions. The setup also included a chin restraint that held the participant's head to the

receiving coil itself. Preliminary inspection of EPI images at the imaging center showed that the setup minimized resting head motion to about 1mm maximum deviation for most subjects.

Diffusion MRI Reconstruction

DSI Studio (http://dsi-studio.labsolver.org) was used to process all DSI images using a q-space diffeomorphic reconstruction method (Yeh & Tseng, 2011). A non-linear spatial normalization approach (Ashburner & Friston, 1999) was implemented through 16 iterations to obtain the spatial mapping function of quantitative anisotropy (QA) values from individual subject diffusion space to the FMRIB 1mm fractional anisotropy (FA) atlas template. QA is an orientation distribution function (ODF) based index that is scaled with spin density information that permits the removal of isotropic diffusion components from the ODF to filter false peaks, facilitating deterministic fiber tractography resolution. For a detailed description and comparison of QA with standard FA techniques, please see Yeh, Verstynen, Wang, Fernández-Miranda, & Tseng, 2013. The ODFs were reconstructed to a spatial resolution of $2mm^3$ with a diffusion sampling length ratio of 1.25. Whole-brain ODF maps of all 60 subjects were averaged to generate a template image of the average tractography space.

Fiber Tractography and Analysis

Fiber tractography was performed using an ODF-streamline version of the FACT algorithm (Yeh et al., 2013) in DSI Studio (September 23, 2013 and August 29, 2014 builds). All fiber tractography was initiated from seed positions with random locations within the wholebrain seed mask with random initial fiber orientations. Using a step size of 1mm, the directional estimates of fiber progression within each voxel were weighted by 80% of the incoming fiber direction and

153 20% of the previous moving direction. A streamline was terminated when the QA index fell
154 below 0.05 or had a turning angle greater than 75°.
155 Fiber tractography was performed in several stages. First, using the group averaged
156 template brain, we tracked 100,000 streamlines that terminated anywhere within a striatal region
157 of interest mask (ROI). To generate this mask, caudate nucleus and putamen masks from the
158 SRI24 multichannel atlas (Rohlfing, Zahr, Sullivan, & Pfefferbaum, 2010) were merged and then
159 expanded by one voxel (2mm) in all directions. This tractography experiment was performed in
160 order to visualize the gradients of connectivity within the striatum (see "Topography of
161 corticostriatal projections" section in Results).
162 After this analysis, we performed ROI-based tractography to isolate streamlines between
163 pairs of ipsilateral cortical and striatal masks. All cortical masks were selected from the SRI24
164 multichannel atlas. Diffusion-based tractography has been shown to exhibit a strong medial bias
165 (Croxson et al., 2005) due to partial volume effects and poor resolution of complex fiber
166 crossings (Jones & Cercignani, 2010). To counter the bias away from more lateral cortical
167 regions, tractography was generated for each cortical surface mask separately. Twenty-six
168 cortical surface masks (13 per hemisphere) in the frontal and parietal lobes were selected from
169 the SRI24 multichannel atlas as targets for corticostriatal tractography, including: gyrus rectus
170 (Rectus); ventromedial prefrontal cortex (Frontal_Med_Orb); opercular, orbital and triangular
171 parts of the inferior frontal gyrus (Frontal_Inf_Oper, Frontal_Inf_Orb, Frontal_Inf_Tri); dorsal
172 and orbital middle and superior frontal gyri (Frontal_Mid, Frontal_Mid_Orb, Frontal_Sup,
173 Frontal_Sup_Orb); superior and inferior parietal lobules (Parietal_Sup, Parietal_Inf); angular
174 gyrus (Angular) and supramarginal gyrus (SupraMarginal). The same striatal ROI mask was
175 used as in the first tractography run. The QA threshold was set to 0.04 for tracking streamlines

176 from the dorsal middle frontal gyri (Frontal_Mid) due to detection of significantly fewer
177 corticostriatal projections than expected (Verstynen, Badre, Jarbo, & Schneider, 2012). Each
178 cortical surface ROI mask was paired with an ipsilateral striatum ROI mask, which were both
179 designated as ends in DSI Studio, and wholebrain seeded tractography continued for $3x10^8$ seeds
180 (approximately 3000 samples per voxel in the whole brain mask). To be included in the final
181 dataset, streamlines had to 1) have a length less than 120mm, and 2) terminate in the cortical
182 surface mask at one end and within the ipsilateral striatum mask at the other. All cortical surface
183 ROI masks were also paired with the contralateral striatum masks. Streamlines were generated
184 for all datasets using the same tracking parameters previously described and a maximum length
185 constraint of 180mm to capture longer interhemispheric projections.

186 Then, to facilitate further analyses, streamlines from the ROI pairings in each hemisphere
187 were combined into three meta-regions. The OFC meta-region was comprised of streamlines
188 from medial and lateral OFC, including: gyrus rectus (Rectus), the orbital part of the inferior
189 frontal gyrus (Frontal_Inf_Orb) and middle (Frontal_Mid_Orb) and superior frontal
190 (Frontal_Sup_Orb) gyri. The DLPFC meta-region consisted of streamlines from opercular
191 (Frontal_Inf_Oper) and triangular (Frontal_Inf_Tri) parts of the inferior frontal gyrus, as well as
192 middle (Frontal_Mid) and superior frontal (Frontal_Sup) gyri. Streamlines from the superior
193 (Parietal_Sup) and inferior parietal lobules (Parietal_Inf), angular gyrus (Angular), and
194 supramarginal gyrus (SupraMarginal) constituted the parietal meta-region. For a more complete
195 assessment of the cortical and striatal topographic organization of the endpoint distributions of
196 the OFC, DLPFC, and parietal meta-regions were reconstructed.

197 In order to confirm the pattern of connectivity observed through the constrained ROI-
198 based approach, a final tractography (Figure 4) analysis was performed by reseeding from a

199 whole-brain mask with each convergence zone designated as an end. This was repeated
200 separately for all four convergence zone masks across all 60 datasets. Tracking proceeded until a
201 total of 50,000 fibers were detected, rather than $3x10^8$ seeds.
202 Approximate motor projections into the striatum were used as a control pathway. These
203 were estimated using the precentral gyrus (Precentral) masks from the SRI24 multichannel atlas.
204 The precentral gyrus masks were designated as endpoint masks paired with ipsilateral and
205 contralateral striatum masks for tracking streamlines using the same parameters described above,
206 across all individual datasets. A single cluster of contiguous voxels was isolated from each
207 putamen in all datasets to create mean striatal precentral clusters.
208
209 *Striatal and Cortical Endpoint Distribution Analysis*
210 The primary tractography variable of interest was the distribution of streamline endpoints. We
211 looked at these endpoints in two separate ways. First, in order to capture the major gradients of
212 corticostriatal pathway organization, we labeled each of the 100,000 streamlines from the first
213 tractography run based on the position of its endpoint within the striatum mask according to two
214 gradients: medial-lateral (x position) and rostral-caudal (y position). Each streamline was then
215 color-coded according to its position in each gradient separately and visualized at the whole
216 brain level (see Figure 1).
217 Next we looked at the distribution of densities of endpoints, across datasets, within each
218 voxel at the subcortical and cortical levels. Custom MATLAB functions were used to generate
219 four striatal endpoint density maps (i.e., convergence zones, see Figures 3 and 4) where all
220 cortical meta-regions yielded overlapping projections within ipsilateral striatum. First, the three-
221 dimensional coordinates of the streamline projection endpoints from each meta-region in the

caudate nucleus and putamen within each hemisphere were extracted. To obtain matrices of striatal endpoint coordinates for each meta-region for all datasets, a mask for each caudate nucleus and putamen were loaded separately into MATLAB with streamlines from each ipsilateral cortical region. A one-sample t-test was used to calculate maps of endpoint densities for each set of streamlines from the individual density maps. Significance was calculated with an FDR-corrected threshold (q) less than 0.05 to identify striatal voxels with projection endpoints from each meta-region that were consistent across all datasets.

Striatal endpoints were then extracted and saved as a new mask, resulting in a three-way convergence zone representing the total volume of contiguous voxels (cluster size $k > 20$) within each nucleus where termination points of projections from the OFC, DLPFC and parietal meta-regions were detected. This was done for both caudate nuclei and putamen resulting in four (left caudate, left putamen, right caudate, and right putamen) convergence zone masks. Convergence zone masks for each nucleus were then used to calculate maps of the mean convergence zone as well as to assess the consistency and significance of convergence zone volumes across all 60 datasets. The significance at each convergence zone was calculated using a one-sample t-test with a $q < 0.05$. For comparison, two-way pairwise convergence zones masks (i.e., OFC + DLPFC, DLPFC + Parietal, and Parietal + OFC) were also created in the same fashion as the three-way convergence zones masks.

After the convergence zones were isolated, cortical endpoints coordinates were extracted from the reseeded tracking described in “Fiber Tractography and Analysis” section. Streamlines between each convergence zone and the wholebrain seed across all datasets were loaded into MATLAB, and the endpoints were saved as masks. A one-sample t-test was conducted to

identify significant voxels throughout the brain that had consistent structural connectivity with each of the convergence zones.

Resting State fMRI Preprocessing and Analyses

SPM8 (Wellcome Department of Imaging Neuroscience, London, UK) was used to preprocess all resting state fMRI data (rsfMRI) collected from 55 of the 60 participants with DSI data. To estimate the normalization transformation for each EPI image, the mean EPI image was first selected as a source image and weighted by its mean across all volumes. Then, an MNI-space EPI template supplied with SPM was selected as the target image for normalization. The source image smoothing kernel was set to a FWHM of 4mm and all other estimation options were kept at the SPM8 defaults to generate a transformation matrix that was applied to each volume of the individual source images for further analyses.

The convergence zones and striatal precentral clusters obtained from the tractography analyses were used as seed points for the functional connectivity analysis. A series of custom MATLAB functions were used to 1) extract the voxel time series of activity for each convergence zone, 2) remove estimated noise from the time series by selecting the first five principle components from the SRI24 tissues white matter and cerebrospinal fluid (CSF) masks, and 3) calculate t and p values of consistent activity with corresponding significance. Resting state fMRI data was analyzed using AFNI (Cox, 1996) to calculate functional activity throughout the brain correlated with each convergence zone and striatal precentral cluster seed in accordance with previously employed methods (see Choi et al., 2012). Specifically, functional activity correlations (r) were converted to *Z*-scores using Fisher's r-to-*Z* transformation for each convergence zone and striatal precentral cluster across all 55 datasets.

First, a convergence zone or striatal precentral cluster mask was loaded into MATLAB 8.1/R2013a (The Mathworks, Sherborn, MA) with an individual participant's rsfMRI time series data. The time series of activity corresponding with the volume of the mask was extracted, yielding activity values for each voxel in the mask across all 210 volumes of the rsfMRI BOLD EPI sequence. Next, the time series was de-noised by regressing the first five principal components of estimated noise from the white matter and CSF voxels out of the total time series activity. Once de-noised, the data were smoothed with a Gaussian kernel (FWHM = 2mm) and a one-sample t-test was run to identify consistent, significant functional activity correlated with the time series across all 55 datasets. Corresponding FDR-corrected values of $q < 0.05$ were also calculated to create maps of significant functional activity for each convergence zone and striatal precentral cluster mask (see Figure 5).

Structural and Functional Connectivity Overlap Analysis

Using a custom MATLAB function, t-maps of consistent structural connectivity from the DSI data, and *Z*-transformed correlation (r) maps from the fMRI data were used to calculate the percentage of structurally significant voxels (i.e., a cortical voxel that had significant structural connectivity with a striatal convergence zone) that were also functionally significant. For this, the DSI t-map data were thresholded at $q < 0.05$ to yield all significant voxels with structural connections that were consistent across all 60 DSI datasets. Corresponding rsfMRI data were also thresholded at $q < 0.05$, resulting in maps of voxels with significant functional connectivity across all 55 fMRI datasets. For each convergence zone, t-maps and *Z*-maps of structural and functional connectivity, respectively, were loaded into MATLAB. A voxel was considered to have significant structural or functional connectivity if the one-sample t-test to find consistent

290 connections across all DSI or rsfMRI datasets resulted in a significant q value. The maps of
291 significant structural and functional connectivity for each convergence zone were binarized such
292 that all voxels with a $q < 0.05$ were set to 1, and all other voxels were set to 0. After transforming
293 the binary data into single column vectors, the dot product of significant structural and functional
294 voxels was summed and divided by the number of significant structural voxels. This calculation
295 yielded the percentage of cortical voxels that had significant structural and functional
296 connectivity with a striatal convergence zone, aggregated across all voxels within a given zone.
297 Finally, a permutation test was conducted to determine the chance levels of overlap
298 between the structural and functional measures of connectivity. For each convergence zone, a
299 random permutation of the resulting binary data vector of significant functional voxels was
300 generated, and the percent overlap with the significant structural voxels was recalculated. This
301 process was repeated for 1000 iterations for each convergence zone ROI to construct the 95%
302 confidence interval of chance overlap between structural and functional connectivity (i.e., to
303 construct the null distribution of structurally connected voxels to the convergence zone that
304 randomly overlapped with functionally connected voxels).
305
306 **Results**
307 *Topography of corticostriatal projections*
308 We first set out to characterize the major topographic gradients of the corticostriatal pathways.
309 While previous animal work using viral tracers (Haber, 2003; Kemp & Powell, 1970; Selemon &
310 Goldman-Rakic, 1985; Utter & Basso, 2008) shows a primarily medial-lateral organization of
311 corticostriatal projections, recent human imaging work suggests a second rostral-to-caudal
312 organization of these pathways (Badre & Frank, 2011; Draganski et al., 2008; Verstynen, Badre,

Jarbo, & Schneider, 2012; Verstynen, 2014). Here, we evaluate the global structural connectivity of the left and right striatum, respectively, on the average template brain. The streamlines are coded according to their position along either a medial-lateral axis (Figure 1A-F) or rostral-caudal axis (Figure 1G-L). Along the medial-lateral axis, we find a gross parcellation between caudate and putamen fibers, with the former receiving projections from rostral prefrontal and orbitofrontal cortex, medial wall areas, and dorsal parietal regions, and the latter receiving projections primarily from somatosensory, primary motor, premotor, and caudal prefrontal areas. Within these major nuclear segmentations, there is a somewhat consistent medial-lateral organization such that more medial areas of cortex project to more medial regions in the subcortical nuclei (cooler colors in Figure 1A-F) and more lateral areas of cortex project to more lateral striatal regions (warmer colors in Figure 1A-F). For example, medial orbitofrontal and ventromedial prefrontal areas project to more medial caudate regions (dark blue) than lateral orbitofrontal cortical streamlines (light blue; see Figure 1C-D). This is largely consistent with previously reported dichotomies of caudate and putamen projections (Alexander et al., 1986) and suggests that at the gross macroscopic level of major cortical regions, the primary gradient of organization is in a medial-to-lateral plane.

The global medial-to-lateral gradient across striatal nuclei is consistent with previous animal imaging studies; however, there is a strong local rostral-caudal organization within the nuclei themselves. Qualitative inspection of Figure 1G-L reveals a rostral-caudal gradient that appears to be isolated within major functionally defined regions. For example, within the lateral prefrontal cortex, that generally tends to project to the putamen (Figure 1A-D), more rostral regions of cortex tend to terminate in more rostral ends of the striatum. However, even this gradient along the sagittal plane segregates some major cortical regions. Motor and

336 somatosensory areas tend to terminate in more caudal regions of the striatum (warmer colors in
337 Figure 1G-L) while prefrontal and orbitofrontal areas terminate in more rostral regions of the
338 striatum (cooler colors in Figure 1G-L). More interestingly, however, parietal projections extend
339 to the more rostral part of the striatum near the location of lateral frontal projection. This is
340 largely consistent with previous animal tracer studies (Cavada & Goldman-Rakic, 1991;
341 Selemon & Goldman-Rakic, 1988) and inconsistent with a pure, global rostral-caudal
342 organization of corticostriatal systems (see Utter & Basso, 2008 for review).

343 These results show that two strong organizational gradients exist in corticostriatal
344 pathways. First, there is a strong macroscopic gradient in a medial-lateral orientation that
345 segregates major functional cortical regions and is moderately driven by spatial proximity. For
346 example, lateral motor areas terminate in the lateral striatal nucleus (i.e., the putamen) and
347 medial motor areas terminate in the more medial nucleus (i.e., the caudate; see Figure 1D).
348 Second, there is a more local gradient in a rostral-caudal direction that is not driven by pure
349 spatial proximity, but appears to reflect local convergence of inputs from disparate cortical
350 regions. An interesting break of this pure rostral-caudal gradient, however, is the observation that
351 parietal streamlines (cyan and light green streamlines in Figure 1G-L) project to rostral portions
352 of the striatum in similar regions as prefrontal and orbitofrontal areas. The location of these
353 parietal projections within both gradients of organization is consistent with parietal inputs
354 converging in similar areas of the striatum as frontal cortex.

355 In order to determine the gross topographic organization across the three major regions of
356 interest for this study, we examined the common regions of endpoint densities in the striatum for
357 all 60 DSI datasets. Thirteen cortical ROIs were tracked and then collapsed into three meta-
358 region maps: OFC, DLPFC, and parietal cortex (see "Methods: Fiber Tractography and

359 Analysis" section for more details). Figure 2 shows the endpoint fields for each meta-region
360 cluster. As expected, the endpoint clusters of projections from the three meta-regions exhibit
361 similar topographical distributions as what is shown in the gradient analysis in Figure 1.
362 Specifically, OFC (yellow) areas project most heavily in the most anterior and medial aspects of
363 the striatum, primarily in the caudate nucleus (Figure 2A). DLPFC (blue, Figure 2B) regions
364 most consistently project just caudal to the OFC clusters and more laterally, although with some
365 visible overlap between the two clusters. Finally, parietal regions (violet, Figure 2C) most
366 densely project to areas slightly more caudal than the DLFPC projections, with a bias towards
367 slightly more lateral striatal regions. This rich, topographical organization of cortical projection
368 endpoints along the striatum demarcates a distinct spatial segmentation of cortical inputs, while
369 also providing evidence of some local overlap of corticostriatal projections from adjacent cortical
370 networks.
371
372 *Convergence of corticostriatal projections*
373 Close inspection of Figure 2 reveals several common regions with apparent overlapping
374 projections from OFC, DLPFC and parietal cortical areas. To quantify these overlapping
375 projections, we used a conjunction analysis to identify voxels with significant endpoint densities
376 from OFC, DLPFC, and parietal masks (see "Materials and Methods"). Clusters of these
377 conjunction voxels ($k > 20$) were isolated bilaterally within the caudate nucleus and putamen
378 separately and were consistent across all 60 datasets (all $t(59)s > 2.75$, $q < 0.05$). Each nucleus
379 contains a distinct cluster of these convergent fields that appear to be relatively symmetric across
380 hemispheres (Figure 3A, left column and Figure 3B). In the caudate, the convergence zones are
381 isolated along the rostral portion of the body of the caudate. In the putamen, the convergence

382 zones are found on the dorsal and rostral aspects of the nucleus. These three-way convergence
383 zones are generally smaller than any of pairwise convergence zones between OFC, DLPFC and
384 parietal cortex. In general, pairwise overlaps with DLPFC are widespread and found across large
385 portions the rostral striatum (Figure 3A, second and third columns). The pairwise overlap of
386 OFC and parietal projections is much smaller (Figure 3A, fourth column), suggesting that the
387 three-way convergence zones are restricted by the limited overlap of parietal and orbitofrontal
388 connections within the striatum. It is important to note that the parietal and OFC overlap areas
389 are away from ventral striatal regions that are typically thought of as the main termini of OFC
390 projections (Haber, 2003). For reference, we also mapped the projections from the precentral
391 gyrus as a proxy for the motor inputs into the striatum, which typically terminate in the caudal
392 putamen (Figure 3A, right column). In all cases, the striatal areas with convergent projections
393 from OFC, DLPFC, and parietal areas is much more rostral than areas that receive projections
394 from precentral motor areas (i.e., the motor striatum).

395 In order to get a more complete picture of where the projections into the striatal
396 convergence zones originate along the cortical surface, we performed a second whole-brain
397 tractography analysis, isolating only streamlines that ended in each of the three-way convergence
398 clusters shown in Figure 3B. While the medial bias of the tractography process is somewhat
399 apparent in this second analysis, we still observed significant structural connectivity from lateral
400 prefrontal and parietal regions. Generally, both putamen convergence zones show more
401 distributed projections (Figure 4: left, red; right, cyan) than the caudate convergence zones
402 projections (Figure 4B: left, blue; right, yellow). The cortical connectivity with the putamen is
403 much more distributed across the frontal and parietal regions than the caudate connectivity.
404 Within OFC, there are two regions with consistent structural connectivity to the convergence

405 zones. The first is a region along the medial wall that connects largely to the putamen
406 convergence zone. The second is a region on the far lateral borders of the OFC, near the border
407 between Brodmann's areas 11 and 47, that shows consistent connectivity to both the caudate and
408 putamen convergence zones. Within the prefrontal cortex, there are two major clusters of
409 connectivity. The first is a cluster on the rostral middle frontal gyrus, approximately at
410 Brodmann's areas 46 and 47, that appears to be contiguous with the lateral OFC clusters and
411 shows a high degree of connectivity with both the caudate and putamen convergence zones. The
412 second, prefrontal cluster rests along the superior frontal gyrus and reflects primarily inputs to
413 the putamen, although a smaller cluster of voxels sends overlapping projections to the caudate.
414 Finally, most projections to the convergence zones from the parietal cortex appear to originate
415 from regions along the angular gyrus and inferior parietal lobule, while some connections within
416 the intraparietal sulcus itself appear to reflect the location of the connections into the caudate
417 convergence zone cluster.

418 Along with connectivity to our three major regions of interest, there is strong connectivity
419 to sensorimotor regions around the precentral sulcus. This is primarily for projections to the
420 putamen convergence zone, although some medial cortical areas show consistent projections to
421 the caudate zone as well. Thus, consistent with the striatal maps in Figure 3A, some sensorimotor
422 regions may also project into rostral portions of the striatal convergence zones, particularly along
423 the putamen.

424 Our original tractography identifying the convergence zones is restricted to ipsilateral
425 corticostriatal projections; however, the reseeded tractography analysis from the left caudate
426 shows several notable interhemispheric connections, particularly with dorsal and medial superior
427 frontal gyrus in the right hemisphere. Contralateral connectivity between left caudate

428 convergence zone and right dorsolateral prefrontal areas is indeed consistent with nonhuman
429 primate histology (McGuire, Bates, & Goldman-Rakic, 1991) and human diffusion imaging
430 work (Lehéricy et al., 2004). No such interhemispheric connectivity is observed from the
431 convergence zone in the right caudate nucleus. However, the lack of strong interhemispheric
432 structural connections may be limited by our initial tractography approach. To correct for this,
433 we conducted a follow-up tractography analysis between convergence zones in one hemisphere
434 and cortical areas in the contralateral hemisphere (see "Methods: Fiber Tractography and
435 Analysis"). After adjusting for multiple comparisons ($q < 0.05$), we did not observe any
436 significant convergence zones from contralateral cortical areas. This null result highlights a
437 limitation of diffusion weighted imaging approaches for tracking contralateral corticostriatal
438 projections previously reported using histological approaches (Cavada & Goldman-Rakic,
439 1989a, 1991; Selemon & Goldman-Rakic, 1985).
440
441 *Functional connectivity of convergence zones*
442 So far our tractography analysis has revealed converging anatomical projections from
443 orbitofrontal, dorsolateral prefrontal and posterior parietal areas into the striatum. If these do, in
444 fact, reflect an integrative functional network, then cortical areas that show a high degree of
445 anatomical connectivity to the convergence zones should also show significant functional
446 connectivity to these same striatal regions. To this end, we used rsfMRI data to measure the
447 functional connectivity between cortical areas and each of the striatal convergence zones. The
448 functional activity of striatal convergence zones is correlated with a distributed set of bilateral
449 cortical areas, including the DLPFC, both medial and lateral OFC, sensorimotor areas, and, most
450 importantly, posterior parietal regions (Figure 5). Within the OFC, we again see that medial

451 regions are more highly connected to the putamen cluster than the caudate cluster, although the
452 functional connectivity appears to be centered in more caudal regions than the location of
453 structural endpoints. The lateral OFC regions, on the border of approximately Brodmann's areas
454 11 and 47, also show connectivity to both convergence zone clusters. This pattern is highly
455 similar to what was observed in the structural connectivity analysis, albeit with a much more
456 distributed cortical representation. In most frontal areas, convergence zones from both nuclei
457 exhibit a similar pattern of functional associations throughout the cortex, particularly in the
458 rostral aspects of the DLPFC, lateral OFC, and anterior cingulate cortex. However, there is also a
459 moderate degree of specificity between the convergence zones on each striatal nucleus. For
460 example, several bilateral cortical regions including the middle frontal gyrus and medial superior
461 frontal gyrus show functional connectivity with only the caudate convergence zones. In contrast,
462 aspects of the precentral gyrus, subgenual cingulate and caudal aspects of the supplementary
463 motor area show unique bilateral connectivity with the convergence zones in the putamen.
464 Functional connectivity with the parietal cortex is restricted along dorsal aspects of the
465 intraparietal sulcus and portions of the inferior parietal lobule. In this case, connectivity to the
466 caudate convergence zone appears to reside in more caudal parietal regions while connectivity to
467 the putamen convergence zone resides in more rostral parietal areas. These regions of unique
468 functional connectivity, along with the unique cortical regions identified in the structural
469 connectivity analysis in Figure 4, suggest that the convergence zones in the caudate nucleus and
470 the putamen may reflect dissociable networks for integrating information from frontoparietal
471 networks.

472 Since the striatal nuclei receive some of the most convergent inputs in the brain (Selemon
473 & Goldman-Rakic, 1985), it is possible that the distributed patterns of functional connectivity

474 that we found to the striatal convergence zones are not unique, but that any striatal area will
475 show a broad and distributed connectivity to many neocortical areas. To address this, we
476 included an additional control analysis looking at the functional connectivity to the motor
477 putamen clusters shown in Figure 3A (right column). The group level functional connectivity to
478 the motor putamen is shown in the center column of Figure 5. As would be expected (see Choi et
479 al., 2012), functional connectivity from the cortex to the motor putamen is quite different than to
480 the convergence zones. There is a much larger representation along the precentral gyrus and
481 central sulcus. While there is a large cluster of connectivity along the medial wall, this cluster is
482 centered much more caudally than the clusters connected to the convergence zones. Some areas
483 do show overlap with the areas that also project to the striatal convergence zones, particularly
484 along the inferior frontal gyrus, which is thought to contain the ventral premotor cortex
485 (Rizzolatti, Fadiga, Gallese, & Fogassi, 1996), as well as some ventral medial wall and ventral
486 parietal areas. However, despite these small regions of overlap, the connectivity patterns of the
487 motor putamen demonstrate that the frontoparietal connectivity found in the convergence zones
488 is not a ubiquitous feature of corticostriatal connections.
489
490 *Structure-function overlap*
491 Comparing the maps in Figures 4 and 5 reveals qualitative similarities in the patterns of
492 structural and functional connectivity to the striatal convergence zones. In order to better
493 understand the similarity between these two connectivity estimates, these maps are plotted
494 together on an inflated brain surface (Figures 6 and 7). Given the relative symmetry of the
495 connectivity patterns between hemispheres, here we will focus on descriptions of ipsilateral
496 connections in the left hemisphere.

On the ventral surface, functional and structural connectivity to the caudate convergence zone overlaps in the same rostral areas of lateral orbital gyrus and ventrolateral inferior frontal gyrus (Figure 6, left panels). However, positive functional connectivity is adjacent to clusters of structural connections in the inferior frontal gyrus and extends caudally to regions that correspond approximately with ventral aspects of Brodmann's area 44 and 45. Functional connectivity to the caudate convergence zone also overlaps with clusters of structural connectivity in caudal regions of the orbital gyrus that extend from inferior frontal gyrus to the medial wall. This functional connectivity appears to be restricted to the same lateral orbital gyrus regions where clusters of structural connections are also present.

Ventral connectivity to the putamen convergence zone shows clusters of structural and functional connections in rostrolateral OFC that extend caudally along the ventral inferior frontal gyrus (Figure 6, upper right). Unlike connections to the caudate convergence zone, structural and functional connections overlap in more central OFC regions as well as throughout ventral aspects of the insula (Figure 6, lower right). Furthermore, large clusters of structural and functional connections to the putamen convergence zone are present along the gyrus rectus. While a much larger swatch of functional connectivity is observed throughout much of the orbital gyrus until the approximate border between medial orbital gyrus and gyrus rectus (Figure 6, lower right), these functional clusters appear to subsume the clusters of structural connections to the putamen convergence zone.

At the lateral surface, there is a high degree of overlap between structural and functional connections to the caudate convergence zone (Figure 7). In DLPFC regions, clusters of structural connections extend caudally from the frontal pole to encompass the rostral two-thirds of the inferior frontal gyrus. Clusters of structural connections are also present along the full extent of

the middle frontal gyrus (Figure 7A, upper left). This spattering of structural connections to the caudate convergence zone overlap with clusters of strong positive functional connectivity in the DLPFC as well (Figure 7A, lower left). In particular, functional connections extend caudally from the frontal pole along the entire inferior frontal gyrus and the rostral third and caudal half of the middle frontal gyrus, overlapping with many of the regions that also show strong structural connections.

Connectivity to the putamen convergence zone appears to be located in similar areas of anterior prefrontal cortex and along the inferior and middle frontal gyri. The main difference between caudate and putamen convergence zone patterns are in the lateral frontal cortex where clusters of structural connections to the putamen are somewhat larger than structural connections to the caudate. Also, the putamen structural connectivity extends more ventrally in the inferior frontal gyrus (Figure 7B, upper left). In the lower left panel of Figure 7B, positive functional connectivity to the putamen convergence zone overlaps with structural connections throughout the inferior frontal gyrus. Small clusters of structural connections appear to overlap with sparse functional connections located in the rostral region of the middle frontal gyrus, contiguous with functional connectivity in rostral superior frontal gyrus; however the structural connections in this region extend much farther back along the middle frontal gyrus than the spread of functional connections.

In parietal areas, an interesting pattern emerges with regards to the specificity connections to the striatal convergence zones. Functionally, the connections to the striatal convergence zones are separated along a dorsal-ventral plane, with patches of negative connectivity present along the superior parietal lobule and dorsal aspects of the intraparietal sulcus and patches of positive connectivity in ventral parietal regions (Figure 7A-B, upper right).

The dorsal negative connectivity region appears to be more distributed for connections to the caudate than to the putamen convergence zone. More importantly, the negative functional connectivity clusters overlap or are physically adjacent to regions of structural connections to both striatal convergence zones (Figure 7A-B, lower right).

For connections to the caudate convergence zone, the positive functional connectivity area in the ventral parietal cortex resides on the border of the supramarginal gyrus and the angular gyrus (Figure 7A, lower right). In contrast, for connections to the putamen convergence zone, this positive connectivity region is shifted in a rostral direction and isolated primarily within the supramarginal gyrus, near the temporal-parietal junction (Figure 7B, lower right). However, here the structural connections do not overlap well with the pattern of functional connections for either convergence zone. We failed to find any structural connections near the positive functional connectivity cluster for the caudate convergence zone. While there is distributed structural connectivity to the putamen convergence zone along the supramarginal and angular gyri, only the most rostral clusters of structural connections appear proximal to the positive functional connectivity region on the supramarginal gyrus. Thus, the only region with consistent structure-function overlaps in the parietal cortex extended along the superior parietal lobule.

Given the incomplete qualitative overlap of structural and functional connectivity, we sought to determine the likelihood that this overlap is due to chance. In order to quantify the degree of overlapping connections, we calculated the probability that structurally connected voxels were also functionally connected, i.e., $P\left(connection_{fMRI} \mid connection_{DSI}\right)$ (see "Methods: Structural and Functional Connectivity Overlap Analysis") and used randomization statistics to estimate the probability of observing this overlap by chance. These results are summarized in

Table 1. The highest degree of overlap was found for the caudate convergence zones. These have the highest degree of specificity of all striatal clusters (i.e., strongest overlap within pairwise maps and weakest connectivity with non-pairwise maps). The functional connectivity of the caudate convergence zones significantly overlap with the structural connectivity of the two putamen clusters, but the degree of this overlap is much smaller than the overlap with the structural connectivity estimated from the caudate convergence zone. Similarly, functional connectivity to the putamen convergence zone overlapped significantly with the structural connectivity to all three striatal clusters; however, unlike the caudate results, the overall degree of overlap was generally smaller and fairly equally distributed across all three striatal clusters. Thus, in both the convergence zone clusters and in both hemispheres, we see a greater degree of overlap in the patterns of functional and structural connectivity than would be expected by chance. In contrast, the control clusters in the motor putamen do not show this pattern. The functional connectivity to the left motor putamen does not significantly overlap with the structural connectivity from any of the striatal clusters in the ipsilateral hemisphere, although the highest degree of overlap was with the structural connectivity patterns to the same set of voxels. The functional connectivity to the right motor putamen only significantly overlapped with the structural connectivity to the same cluster of voxels, but not to the structural connectivity maps to either of the convergence zones. This overlap of functional and structural connectivity patterns in the cortex provides confirmation that voxels showing direct anatomical connections to the striatal convergence zones have a high likelihood—well above chance—of being associated in their functional dynamics. Furthermore, the cortical distribution of inputs to the convergence zones reflects a unique set of frontoparietal networks and not a general pattern of corticostriatal connectivity.

Discussion

Our results identify a novel set of regions in the rostral and dorsal striatum that concurrently exhibit structural and functional connectivity to orbitofrontal, dorsolateral prefrontal, and posterior parietal regions of cortex. The location of these convergence zones is anatomically consistent with previous reports of parietal (Cavada & Goldman-Rakic, 1991; Selemon & Goldman-Rakic, 1985, 1988) and frontal (Averbeck et al., 2014; S. Haber, Kunishio, Mizobuchi, & Lynd-Balta, 1995) white matter projections, based on ex-vivo nonhuman primate histology. While the distribution of cortical regions associated with the striatal convergence zones differed to some degree between structural and functional connectivity measures, reflecting methodological limitations of each approach, a majority of cortical areas structurally connected to the convergence zones also showed strong functional connectivity. This supports the notion that these corticostriatal projections form an integrative functional circuit.

The current findings support a growing body of evidence that basal ganglia circuits are more complex and interactive than the classic independent, parallel pathways model (Alexander et al., 1986). We confirmed the presence of two previously described gradients of connectivity within the corticostriatal pathways: a global medial-lateral gradient.(Haber, 2003; Selemon & Goldman-Rakic, 1985), and a more local rostral-caudal gradient (Kemp & Powell, 1970; Whitlock & Nauta, 1956; see also Draganski et al., 2008; Verstynen, Badre, Jarbo, & Schneider, 2012). The complexity of these gradients highlights the fact that demarcating independent corticostriatal circuits remains a challenge (see also Choi et al., 2012).

Histological work has also shown that corticostriatal pathways from disparate cortical areas have some overlapping termination fields within the striatum (Averbeck et al., 2014;

612 Haber, Kim, Mailly, & Calzavara, 2006; Haber, 2003; Selemon & Goldman-Rakic, 1985).
613 Accordingly, we observed clusters of voxels (i.e., convergence zones) bilaterally within striatal
614 nuclei where projections from several cortical areas including OFC, DLPFC, and posterior
615 parietal cortex terminate. This is in line with recent work in humans showing that distinct striatal
616 regions are functionally connected with networks of distributed cortical areas including the
617 frontoparietal association, default mode, and limbic networks (Choi et al., 2012). While previous
618 work has separately shown projections from OFC (Haber et al., 2006; Selemon & Goldman-
619 Rakic, 1985) and posterior parietal cortex (Cavada & Goldman-Rakic, 1989, 1991; Selemon &
620 Goldman-Rakic, 1988) overlap with DLPFC projections, to the best of our knowledge the
621 present findings show the first evidence of a convergence of projections from all three cortical
622 areas to common striatal targets.
623 We propose that this pattern of convergent connectivity may reflect a potential
624 mechanism for integrating reward processing, executive control, and spatial attention during
625 spatial reinforcement learning (Behrmann, Geng, & Shomstein, 2004; Colby & Goldberg, 1999;
626 Gottlieb, 2007). This type of learning is thought to arise from feedback signals refining
627 behavioral action selections and strategies, in order to improve efficiency during visual search
628 for highly rewarded spatial targets versus targets that are less rewarded (Della Libera &
629 Chelazzi, 2006; Kristjansson et al., 2010; Lee & Shomstein, 2014; Navalpakkam, Koch, Rangel,
630 & Perona, 2010). At the neural level, performance on spatial reinforcement tasks has been shown
631 to be associated with concurrent activity of posterior parietal and DLPFC areas (Lee &
632 Shomstein, 2013); however, in order for feedback to bias spatial attention, signals from cortical
633 areas linked to attention must be integrated with reinforcement learning processes, i.e.,
634 evaluating previous outcomes and using them to shape response selection. Functionally, the

orbitofrontal cortex has been implicated in providing reinforcement signals that influence behavior (Hare, O'Doherty, Camerer, Schultz, & Rangel, 2008; O'Doherty, 2004; Schoenbaum, Roesch, Stalnaker, & Yuji, 2010). Thus, convergence of orbitofrontal signals into regions of the striatum that also receive projections from cortical areas linked to spatial attention and executive control could provide a substrate for adapting spatial decisions.

The dual location of the projections from the orbitofrontal cortex into the striatal convergence zones may also help to elucidate the role of feedback control in spatial learning. Orbitofrontal areas have a well-described dual topography of representation: one for sensory modality and feedback type (i.e., reward and punishment), and another for complexity of feedback information (for complete review, see Kringelbach & Rolls, 2004). We observed two distinct clusters of orbitofrontal projections into the convergence zones that illustrate this dual topography (see Figure 4, bottom row center). The larger cluster of projections to both striatal nuclei was found in posterior lateral orbitofrontal areas that are linked with processing low complexity visual signals. This supports the idea that these projections are linked to processing signals necessary for visuospatial attention. The second, smaller, cluster of projections originated in anterior medial regions and terminated only within the putamen convergence zones. These may reflect subsets of projections to pure ventral striatal pathways linked directly to reward processing (e.g., the ventral parts of the putamen clusters illustrated in Figure 3, left column), suggesting that these striatal convergence zones may reflect multiple forms of feedback processing during spatial learning.

Within the striatal nuclei, the location of the convergence zones also provides some clues as to the possible functional roles of these integrative networks. For example, we observed convergence zones that extended into the dorsomedial caudate nucleus. This area has been

658 strongly implicated in reinforcement learning in human functional neuroimaging studies (Badre
659 & Frank, 2012; Daw, Joel, & Doherty, 2007; Delgado et al., 2005; O'Doherty et al., 2004;
660 Schönberg, Daw, Joel, & O'Doherty, 2007). When these previous studies are considered together
661 with our coincidental observation of structural and functional connectivity between OFC,
662 DLPFC, and posterior parietal cortex and the striatum, the convergence of these three
663 corticostriatal pathways, particularly within the dorsomedial caudate, may underlie context-
664 dependent, spatial reinforcement learning suggested in previous research (Lee & Shomstein,
665 2013; Nieuwenhuis, Slagter, von Geusau, Heslenfeld, & Holroyd, 2005; Nieuwenhuis,
666 Heslenfeld, et al., 2005).

667 Of course, it is possible that at least part of the interaction between parietal, OFC and
668 DLPFC functions is mediated by direct intracortical structural connections (Ridderinkhof, van
669 den Wildenberg, Segalowitz, & Carter, 2004); however, our current findings are consistent with
670 a model in which part of this integration may happen at the corticostriatal level (Haber et al.,
671 2006). Similarly, histological work supports potential models of spatial attention and executive
672 control integration via direct cortical connections between posterior parietal cortex and DLPFC
673 (Cavada & Goldman-Rakic, 1989b), as well as overlapping corticostriatal projections (Cavada &
674 Goldman-Rakic, 1991). While we cannot rule out a direct cortico-cortical connectivity
675 hypothesis, our findings afford some confirmation for the integration of spatial attention and
676 executive control signals in striatal areas that also receive inputs from the OFC, which is
677 consistent with a corticostriatal mechanism for spatial reinforcement learning.

678 Our conclusions about this pathway are tempered, however, by inherent methodological
679 limitations with the neuroimaging techniques that we used. The low spatial resolution of current
680 MRI techniques (2-3mm^3 voxels), relative to histological approaches, means that it is not

681 possible to directly infer whether the pathways we visualized are converging on the same striatal
682 cells or merely terminating in adjacent regions of the nucleus. Even considering that it is possible
683 to get sub-voxel resolution with tractography on diffusion imaging data (Verstynen et al., 2012;
684 Verstynen, Jarbo, Pathak, & Schneider, 2011), this resolution is simply not fine enough to detect
685 true converging collaterals on the same neuron. This coarse resolution of current MRI-based
686 approaches limits our inference to interactions that occur at the voxel level.

687 Another concern relates generally to rsfMRI functional connectivity analyses, which is an
688 indirect measure of connectivity based on correlated activity throughout the brain. At the time-
689 scale of the BOLD response it is impossible to differentiate direct functional connections to a
690 seed region from indirect connections (Cole, Smith, & Beckmann, 2010). Thus, our inferences
691 based on rsfMRI data can only imply that connected regions represent a functional circuit, but
692 they cannot confirm that correlated areas are directly connected to each other. While fiber
693 tractography provides a more direct estimate of underlying white matter connections, this
694 approach is still highly sensitive to various sources of noise (Jones, 2008) and suffers from
695 several spatial biases that preclude complete identification of all underlying connectivity (see
696 Thomas et al., 2014). This bias may explain some of the discrepancies between the structural
697 (Figure 4) and functional (Figure 5) connectivity patterns in the present study, particularly in
698 DLPFC regions.

699 Finally, neither DSI nor rsfMRI can confirm the task-relevance of the cortical areas that
700 we examined. In order to directly address our hypothesis that this network reflects a neural
701 substrate for spatial reinforcement learning, future work should look at functions of this network
702 during tasks that require the integration of reward, executive control, and spatial attention.

In spite of these limitations, the present findings provide clear evidence that projections from OFC, DLPFC, and posterior parietal cortex terminate in common striatal regions. While our results are consistent with several independent findings in primate neuroanatomical literature, no previous study has shown the specific convergence of these three corticostriatal pathways in the human brain. This highlights a plausible structural mechanism that could allow for parietally-mediated spatial attention processes to contribute to the integration of reward and response selection. Future work should explore the particular dynamics of the neural circuit that we have described here for their potential role in the integration of spatial attention information with reward and executive control processes during reinforcement learning.

References

Alexander, G. E., DeLong, M. R., & Strick, P. L. (1986). Parallel organization of functionally segregated circuits linking basal ganglia and cortex. *Annual Review of Neuroscience*, *9*, 357–381.

Ashburner, J., & Friston, K. J. (1999). Nonlinear Spatial Normalization Using Basis Funcitons. *Human Brain Mapping*, *7*, 254–266.

Averbeck, B. B., Lehman, J., Jacobson, M., & Haber, S. N. (2014). Estimates of Projection Overlap and Zones of Convergence within Frontal-Striatal Circuits. *Journal of Neuroscience*, *34*(29), 9497–9505.

Badre, D., & Frank, M. J. (2012). Mechanisms of hierarchical reinforcement learning in cortico-striatal circuits 2: evidence from fMRI. *Cerebral Cortex*, *22*(3), 527–36. doi:10.1093/cercor/bhr117

Behrmann, M., Geng, J. J., & Shomstein, S. (2004). Parietal cortex and attention. *Current Opinion in Neurobiology*, *14*(2), 212–7.

Cavada, C., & Goldman-Rakic, P. S. (1989a). Posterior parietal cortex in rhesus monkey: I. Parcellation of areas based on distinctive limbic and sensory corticocortical connections. *The Journal of Comparative Neurology*, *287*(4), 393–421.

Cavada, C., & Goldman-Rakic, P. S. (1989b). Posterior parietal cortex in rhesus monkey: II. Evidence for segregated corticocortical networks linking sensory and limbic areas with the frontal lobe. *The Journal of Comparative Neurology*, *287*(4), 422–45.

Cavada, C., & Goldman-Rakic, P. S. (1991). Topographic segregation of corticostriatal projections from posterior parietal subdivisions in the macaque monkey. *Neuroscience*, *42*(3), 683–96.

Choi, E. Y., Yeo, B. T. T., & Buckner, R. L. (2012). The organization of the human striatum estimated by intrinsic functional connectivity. *Journal of Neurophysiology*, *108*(8), 2242–63.

Colby, C. L., & Goldberg, M. E. (1999). Space and Attention in Partietal Cortex. *Annual Review of Neuroscience*, *22*, 319–49.

Cole, D. M., Smith, S. M., & Beckmann, C. F. (2010). Advances and pitfalls in the analysis and interpretation of resting-state FMRI data. *Frontiers in Systems Neuroscience*, *4*, 8.

Cox, R. W. (1996). AFNI: Software for Analysis and Visualization of Functional Magnetic Resonance Neuroimages. *Computers and Biomedical Research*, *29*(3), 162–173.

Critchely, M. (1953). The parietal lobes. Oxford, England: Williams and Wilkins

Croxson, P. L., Johansen-Berg, H., Behrens, T. E. J., Robson, M. D., Pinsk, M., Gross, C. G., Rushworth, M. F. S. (2005). Quantitative investigation of connections of the prefrontal cortex in the human and macaque using probabilistic diffusion tractography. *Journal of Neuroscience 25*(39), 8854–66.

Daw, N. D., & Doya, K. (2006). The computational neurobiology of learning and reward. *Current Opinion in Neurobiology*, *16*(2), 199–204.

Daw, N. D., Joel, D., & Doherty, J. P. O. (2007). Reinforcement Learning Signals in the Human Striatum Distinguish Learners from Nonlearners during Reward-Based Decision Making. *The Journal of Neuroscience*, *27*(47), 12860–12867.

Dayan, P., & Abbott, L. F. (2001). *Theoretical Neuroscience: Computational and Mathematical Modeling of Neural Systems* (1st ed.). Cambridge, MA: MIT Press.

Delgado, M. R., Locke, H. M., Stenger, V. a, & Fiez, J. a. (2003). Dorsal striatum responses to reward and punishment: effects of valence and magnitude manipulations. *Cognitive, Affective & Behavioral Neuroscience*, *3*(1), 27–38.

Delgado, M. R., Miller, M. M., Inati, S., & Phelps, E. A. (2005). An fMRI study of reward-related probability learning. *NeuroImage*, *24*(3), 862–73.

Della Libera, C., & Chelazzi, L. (2006). Visual selective attention and the effects of monetary rewards. *Psychological Science*, *17*(3), 222–7.

Di Martino, A., Scheres, A., Margulies, D. S., Kelly, A. M. C., Uddin, L. Q., Shehzad, Z., … Milham, M. P. (2008). Functional connectivity of human striatum: a resting state FMRI study. *Cerebral Cortex*, *18*(12), 2735–47.

Draganski, B., Kherif, F., Klöppel, S., Cook, P. a, Alexander, D. C., Parker, G. J. M., Frackowiak, R. S. J. (2008). Evidence for segregated and integrative connectivity patterns in the human Basal Ganglia. *The Journal of Neuroscience*, *28*(28), 7143–52.

Egeth, H. E., & Yantis, S. (1997). Visual attention: control, representation, and time course. *Annual Review of Psychology*, *48*, 269–97.

Gottlieb, J. (2007). From thought to action: the parietal cortex as a bridge between perception, action, and cognition. *Neuron*, *53*(1), 9–16.

Graybiel, A. M. (1995). Building action repertoires: memory and learning functions of the basal ganglia. *Current Opinion in Neurobiology*, *5*(6), 733–41.

Haber, S. N., Kunishio, K., Mizobuchi, M., & Lynd-Balta, E. (1995). The orbital and medial prefrontal circuit through the primate basal ganglia. *The Journal of Neuroscience*, *15*(7), 4851–4867.

Haber, S. N. (2003). The primate basal ganglia: parallel and integrative networks. *Journal of Chemical Neuroanatomy*, *26*(4), 317–330.

Haber, S. N., Kim, K. S., Mailly, P., & Calzavara, R. (2006). Reward-related cortical inputs define a large striatal region in primates that interface with associative cortical connections, providing a substrate for incentive-based learning. *The Journal of Neuroscience*, *26*(32), 8368–76.

Haber, S. N., & Knutson, B. (2010). The reward circuit: linking primate anatomy and human imaging. *Neuropsychopharmacology*, *35*(1), 4–26.

Hare, T. A., O'Doherty, J., Camerer, C. F., Schultz, W., & Rangel, A. (2008). Dissociating the role of the orbitofrontal cortex and the striatum in the computation of goal values and prediction errors. *The Journal of Neuroscience*, *28*(22), 5623–30.

Jones, D. K. (2008). Special issue : Original article Studying connections in the living human brain with diffusion MRI. *Cortex*, *44*, 936–952.

Jones, D. K., & Cercignani, M. (2010). Twenty-five pitfalls in the analysis of diffusion MRI data. *NMR in Biomedicine*, *23*(7), 803–20.

Kemp, J. M., & Powell, T. P. S. (1970). The Cortico-Striate Projections in the Monkey. *Brain*, *93*, 525–46.

Knutson, B., & Cooper, J. C. (2005). Functional magnetic resonance imaging of reward prediction. *Current Opinion in Neurology*, 1–8.

Knutson, B., Westdorp, A., Kaiser, E., & Hommer, D. (2000). fMRI visualization of brain activity during a monetary incentive delay task. *NeuroImage*, *12*(1), 20–7.

Kringelbach, M. L., & Rolls, E. T. (2004). The functional neuroanatomy of the human orbitofrontal cortex: evidence from neuroimaging and neuropsychology. *Progress in Neurobiology*, *72*(5), 341–72.

Kristjansson, A., Sigurjonsdottir, O., & Driver, J. (2010). Fortune and reversals of fortune in visual search: Reward contingencies for pop-out targets affect. *Attention, Perception & Psychophysics*, *72*(5), 1229–1236.

Kuhnen, C. M., & Knutson, B. (2005). The neural basis of financial risk taking. *Neuron*, *47*(5), 763–70.

Lee, J., & Shomstein, S. (2013). The differential effects of reward on space- and object-based attentional allocation. *The Journal of Neuroscience*, *33*(26), 10625–33.

Lee, J., & Shomstein, S. (2014). Reward-based transfer from bottom-up to top-down search tasks. *Psychological Science*, *25*(2), 466–75.

Lehéricy, S., Ducros, M., Krainik, A., Francois, C., Van de Moortele, P.-F., Ugurbil, K., & Kim, D.-S. (2004). 3-D diffusion tensor axonal tracking shows distinct SMA and pre-SMA projections to the human striatum. *Cerebral Cortex*, *14*(12), 1302–9.

Lohrenz, T., McCabe, K., Camerer, C. F., & Montague, P. R. (2007). Neural signature of fictive learning signals in a sequential investment task. *Proceedings of the National Academy of Sciences of the United States of America*, *104*(22), 9493–8.

Mcclure, S. M., York, M. K., & Montague, P. R. (2004). The Neural Substrates of Reward Processing in Humans : The Modern Role of fMRI. *The Neuroscientist*, *10*(3), 260–268.

McGuire, P. K., Bates, J. F., & Goldman-Rakic, P. S. (1991). Interhemispheric Integration: II. Symmetry and Convergence of the Corticostriatal Projections of the Left and the Right Principal Sulcus (PS) and the Left and the Right Supplementary Motor Area (SMA) of the Rhesus Monkey. *Cerebral Cortex*, *1*(5), 408–417.

Navalpakkam, V., Koch, C., Rangel, A., & Perona, P. (2010). Optimal reward harvesting in complex perceptual environments. *Proceedings of the National Academy of Sciences of the United States of America*, *107*(11), 5232–7.

Nieuwenhuis, S., Heslenfeld, D. J., Alting von Geusau, N. J., Mars, R. B., Holroyd, C. B., & Yeung, N. (2005). Activity in human reward-sensitive brain areas is strongly context dependent. *NeuroImage*, *25*(4), 1302–1309.

Nieuwenhuis, S., Slagter, H. A., von Geusau, N. J. A., Heslenfeld, D. J., & Holroyd, C. B. (2005). Knowing good from bad: differential activation of human cortical areas by positive and negative outcomes. *The European Journal of Neuroscience*, *21*(11), 3161–8.

O'Doherty, J. P., Dayan, P., Friston, K. J., Critchley, H., & Dolan, R. J. (2003). Temporal Difference Models and Reward-Related Learning in the Human Brain. *Neuron*, *28*, 329–337.

O'Doherty, J., Dayan, P., Schultz, J., Deichmann, R., Friston, K., & Dolan, R. J. (2004). Dissociable roles of ventral and dorsal striatum in instrumental conditioning. *Science*, *304*(5669), 452–4.

O'Doherty, J. P. (2004). Reward representations and reward-related learning in the human brain : insights from neuroimaging. *Current Opinion in Neurobiology*, 769–776.

Pagnoni, G., Zink, C. F., Montague, P. R., & Berns, G. S. (2002). Activity in human ventral striatum locked to errors of reward prediction. *Nature Neuroscience*, *5*(2), 97–8.

Posner, M. I., Snyder, C. R., & Davidson, B. J. (1980). Attention and the detection of signals. *Journal of Experimental Psychology*, *109*(2), 160–74.

Ridderinkhof, K. R., van den Wildenberg, W. P. M., Segalowitz, S. J., & Carter, C. S. (2004). Neurocognitive mechanisms of cognitive control: the role of prefrontal cortex in action selection, response inhibition, performance monitoring, and reward-based learning. *Brain and Cognition*, *56*(2), 129–40.

Rizzolatti, G., Fadiga, L., Gallese, V., & Fogassi, L. (1996). Premotor cortex and the recognition of motor actions. *Cognitive Brain Research*, *3*(2), 131–41.

Rodriguez, P. F., Aron, A. R., & Poldrack, R. A. (2006). Ventral-striatal/nucleus-accumbens sensitivity to prediction errors during classification learning. *Human Brain Mapping*, *27*(4), 306–13.

Rohlfing, T., Zahr, N. M., Sullivan, E. V, & Pfefferbaum, A. (2010). The SRI24 multichannel atlas of normal adult human brain structure. *Human Brain Mapping*, *31*(5), 798–819.

Schoenbaum, G., Roesch, M. R., Stalnaker, T. A., & Yuji, K. (2010). A new perspective on the role of the orbitofrontal cortex in adaptive behaviour. *Nature Neuroscience Reviews*, *10*(12), 885–892.

Schönberg, T., Daw, N. D., Joel, D., & O'Doherty, J. P. (2007). Reinforcement learning signals in the human striatum distinguish learners from nonlearners during reward-based decision making. *The Journal of Neuroscience : The Official Journal of the Society for Neuroscience*, *27*(47), 12860–7.

Selemon, L. D., & Goldman-Rakic, P. S. (1985). Longitudinal Topography and lnterdigitation of Corticostriatal Projections in the Rhesus Monkey. *Journal of Neuroscience*, *5*(3), 776–794.

Selemon, L. D., & Goldman-Rakic, P. S. (1988). Common cortical and subcortical targets of the dorsolateral prefrontal and posterior parietal cortices in the rhesus monkey: evidence for a distributed neural network subserving spatially guided behavior. *The Journal of Neuroscience*, *8*(11), 4049–68.

Silver, M. A., Ress, D., & Heeger, D. J. (2005). Topographic maps of visual spatial attention in human parietal cortex. *Journal of Neurophysiology*, *94*(2), 1358–71.

Sutton, R. S., & Barto, A. G. (1998). Introduction to Reinforcement Learning. Cambrige, MA: MIT Press.

Thomas, C., Ye, F. Q., Irfanoglu, M. O., Modi, P., Saleem, K. S., Leopold, D. A., & Pierpaoli, C. (2014). Anatomical accuracy of brain connections derived from diffusion MRI tractography

is inherently limited. *Proceedings of the National Academy of Sciences*, *111*(46), 16574–16579.

Utter, A., & Basso, M.. (2008). The basal ganglia: an overview of circuits and function. *Neuroscience and Biobehavioral Reviews*, *32*(3), 333–42.

Verstynen, T. D. (2014). The organization and dynamics of corticostriatal pathways link the medial orbitofrontal cortex to future behavioral responses. *Journal of Neurophysiology*, *112*(10), 2457–69.

Verstynen, T. D., Badre, D., Jarbo, K., & Schneider, W. (2012). Microstructural organizational patterns in the human corticostriatal system. *Journal of Neurophysiology*, *107*, 2984–2995.

Verstynen, T. D., Jarbo, K., Pathak, S., & Schneider, W. (2011). In Vivo Mapping of Microstructural Somatotopies in the Human Corticospinal Pathways In Vivo Mapping of Microstructural Somatotopies in the Human Corticospinal Pathways. *Journal of Neurophysiology*, *105,* 336–346.

Whitlock, D., & Nauta, W. (1956). Subcortical Projections from the Temporal Neocortex in Macaca Mulatta. *Journal of Comparative Neurology, 106*(1), 183-212.

Yeh, F., & Tseng, W. I. (2011). NTU-90: a high angular resolution brain atlas contructed by q-space diffeomorphic reconstruction. *NeuroImage*, *58*(1), 91–99.

Yeh, F., Verstynen, T. D., Wang, Y., Fernández-Miranda, J. C., & Tseng, W.Y. I. (2013). Deterministic Diffusion Fiber Tracking Improved by Quantitative Anisotropy. *PLoS ONE*, *8*(11), e80713.

Figures

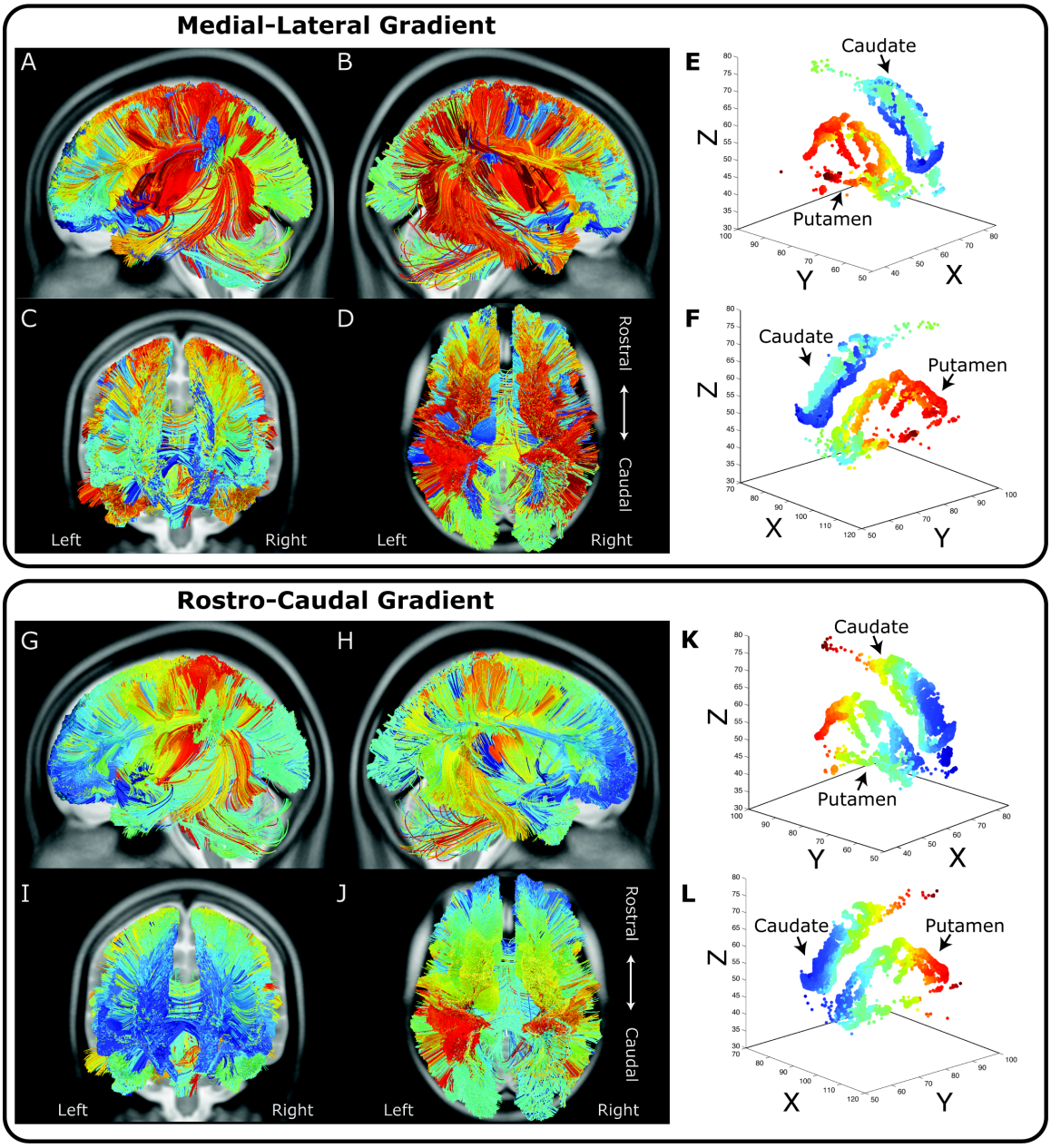

Figure 1. Tractography analysis of medial-lateral (A-F) and rostral-caudal (G-L) striatal topography in the average participant template brain. Streamlines were tracked from whole-brain seeds to caudate and putamen masks. In panels A-F, cooler colors indicate streamlines that terminate more medially, while warmer colors indicate those that terminate more laterally. Along medial-lateral orientation, spatially proximal cortical areas project to similar locations within the

striatum. In panels G-L, cooler and warmer colors indicate streamlines that terminate in more rostral and caudal striatal areas, respectively.

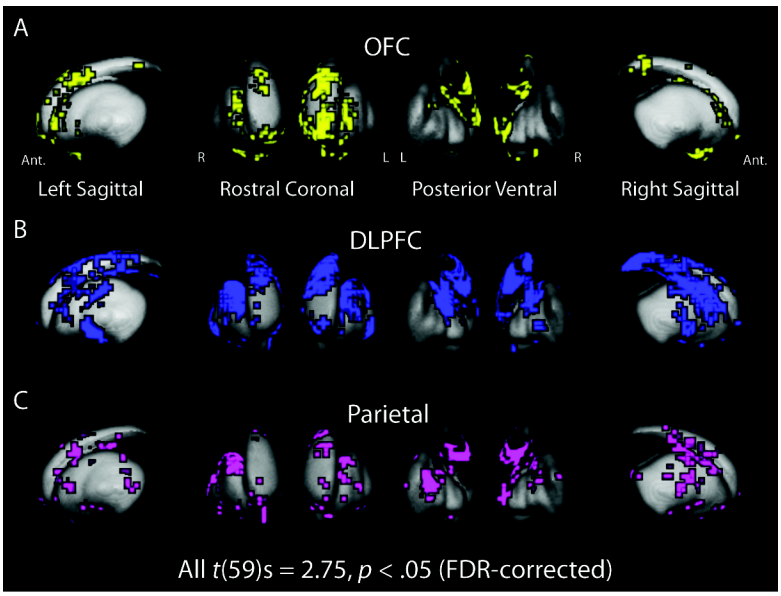

Figure 2. Group statistical maps of common endpoint locations from three cortical meta-regions: orbitofrontal cortex (OFC; yellow), dorsolateral prefrontal cortex (DLPFC; blue) and parietal cortex (violet). Voxels indicate regions with significant endpoint densities from cortex determined using a 1-sample t-test and corrected for multiple comparisons.

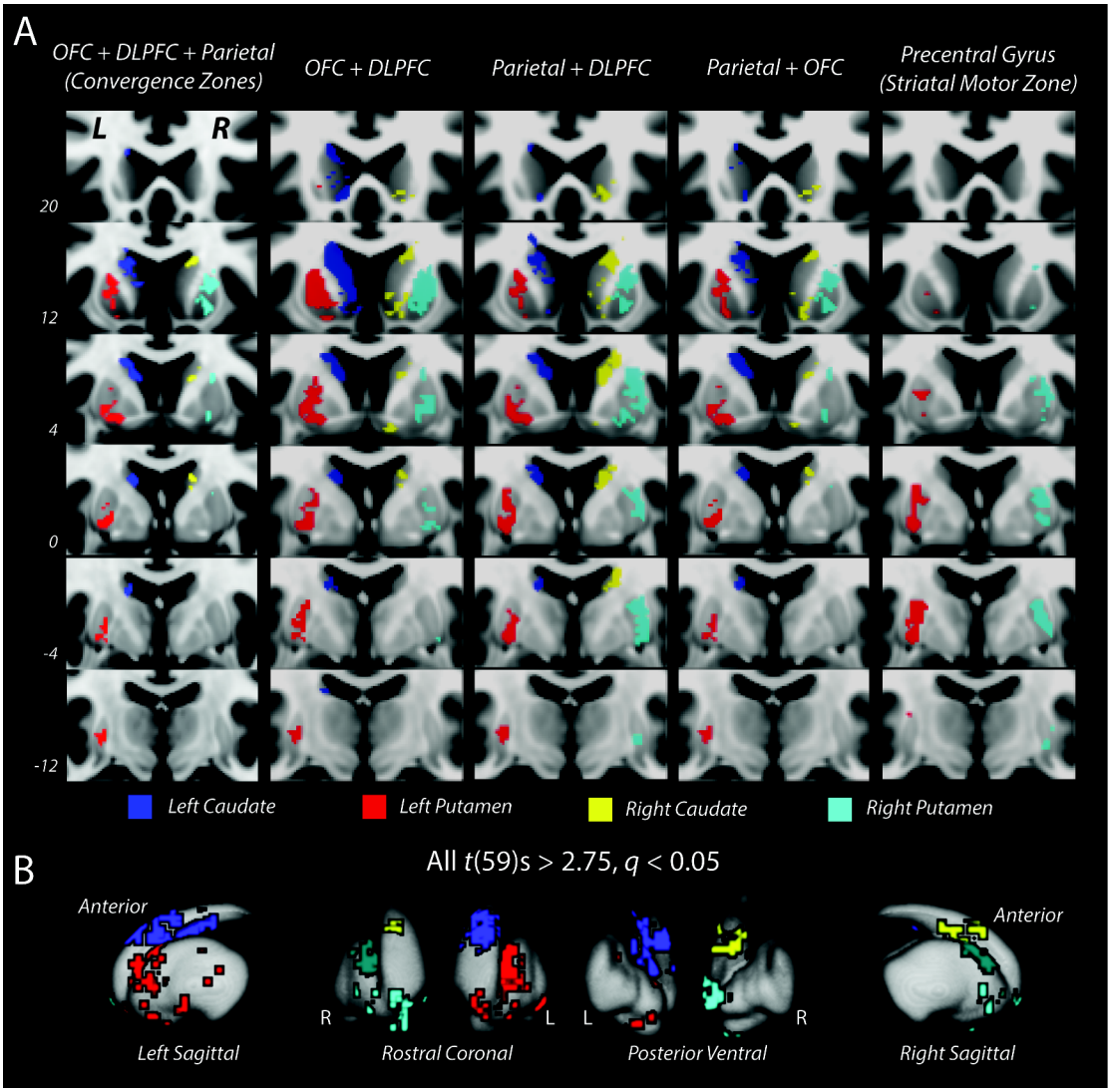

Figure 3. Coronal slice images and 3D representations of mean convergence and non-convergence zone masks within bilateral caudate nucleus and putamen. A) Coronal slice view of three-way (left column) and two-way (middle three columns) convergence zone, and striatal motor (right column) non-convergence zones masks on T1-weighted MNI-space brain. Three-way and two-way convergence zones (four left columns) were isolated in both striatal nuclei bilaterally: left caudate = blue, left putamen = red, right caudate = yellow, right putamen = cyan. Non-convergence zones (right column) are restricted to regions of putamen (left = red, right = cyan) that received projections from ipsilateral precentral gyrus. All striatal masks consist of

single clusters of significant (all $t(59)s > 2.75$, FDR-corrected $q < 0.05$) contiguous voxels (cluster size $k > 20$) with streamline endpoints from the cortical areas indicate above each column. Three-way convergence zones are smaller in volume than two-way convergence zones and are located more rostrally in striatal nuclei than non-convergence zones. B) 3D surface visualizations of three-way convergence zones.

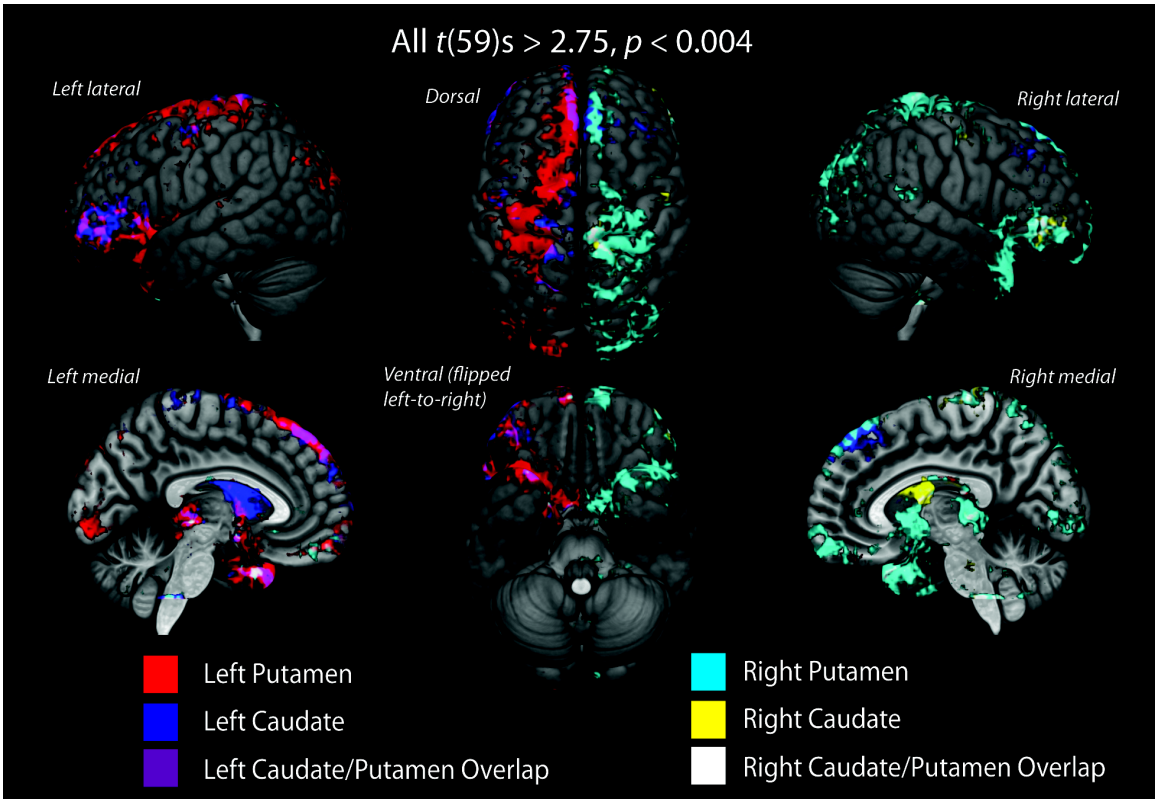

Figure 4. Cortical endpoint density maps of tractography into each convergence zone mask on template brain. Streamlines were tracked from a wholebrain seed to individual three-way convergence zone masks. Maps show cortical and subcortical regions with consistent (all t(59)s > 2.75, uncorrected p < 0.004) endpoint projections into each convergence zone (left caudate = blue, left putamen = red, right caudate = yellow, right putamen = cyan) across all subjects. Connections with the putamen convergence zone originate from a much larger and more distributed set of cortical areas than those with caudate convergence zone. Overlapping structural connectivity from ipsilateral caudate and putamen convergence zones in orbitofrontal, dorsolateral prefrontal, and parietal cortex areas between is shown as purple in left hemisphere and white in right hemisphere.

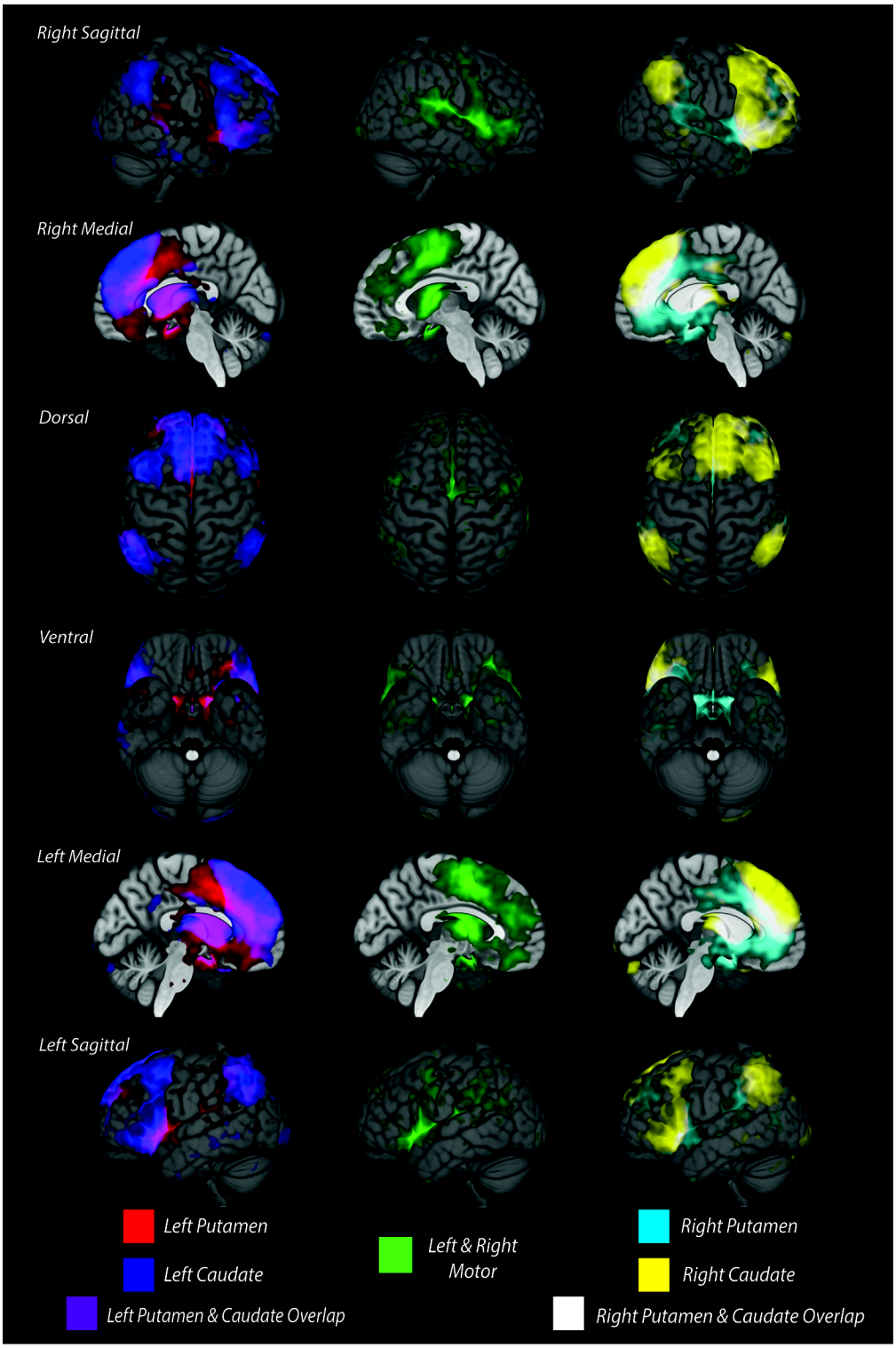

Figure 5. Resting state fMRI maps of functional connectivity of convergence and non-convergence zones with the whole brain after adjusting for multiple comparisons. Correlations

from individual resting state datasets (N =55) were normalized using Fisher's r-to-Z transformation and group maps were calculated using a one-sample t-test with an FDR-corrected q value < 0.05. Both caudate convergence zone maps were thresholded at Z(r) = 0.03-0.10, and putamen convergence and non-convergence zone maps were thresholded at Z(r) = 0.05-0.10. Overlaid cortical activity patterns show correlated functional connectivity with the left (left column; caudate = blue, putamen = red) and right (right column; caudate = yellow, putamen = cyan) convergence zones and bilateral non-convergence zones in striatal motor regions of the putamen (middle column; green) separately. Significant functional connectivity of ipsilateral caudate and putamen convergence zones overlap in orbitofrontal, dorsolateral prefrontal, and parietal areas laterally, and in anterior cingulate cortex medially. Non-convergence zone functional connectivity is primarily restricted to precentral gyrus and insular cortex laterally, and some anterior cingulate cortex and caudal superior frontal gyrus medially.

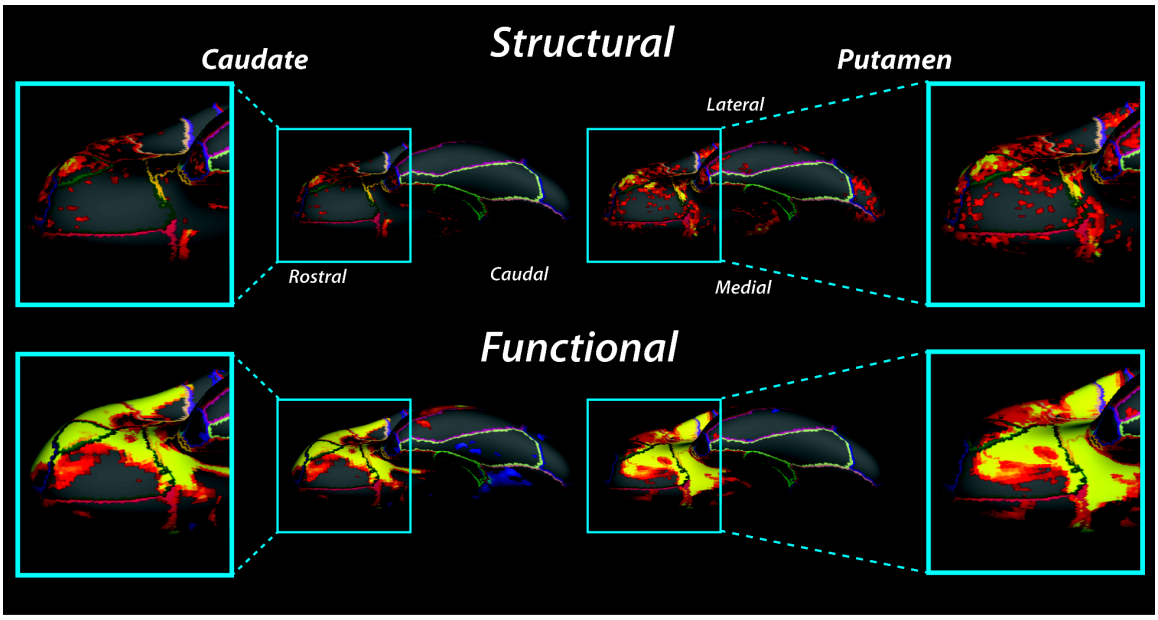

Figure 6. Ventral surface maps of structural and functional convergence zone connectivity in orbitofrontal cortex on an inflated brain. Clusters of significant (all t's > 2.75, uncorrected $p < 0.05$) structural and functional connectivity are observed to overlap throughout orbitofrontal cortex. Warmer colors indicate $t > 2.75$; cooler colors indicate $t < -2.75$. Connectivity to the caudate convergence zone is depicted in the left panels and connectivity to the putamen convergence zone is depicted in the right panels.

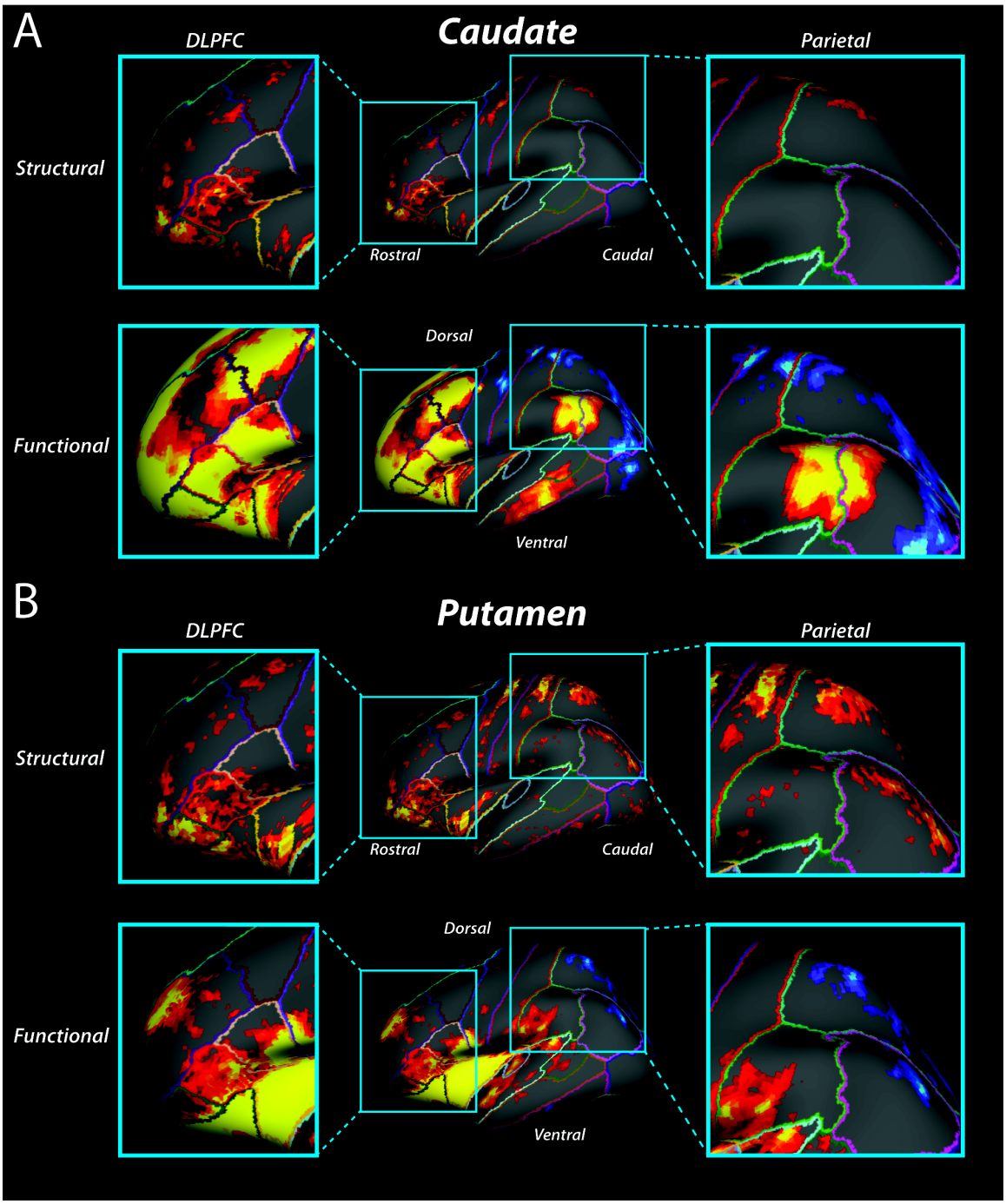

Figure 7. Lateral surface maps of structural and functional convergence zone connectivity in dorsolateral prefrontal and parietal cortex on an inflated brain. A) Connectivity to the caudate convergence zone. B) Connectivity to the putamen convergence zone. Same plotting conventions as in Figure 6.

Table 1. Observed structural and functional overlap probabilities within and across the two convergence zones and connections to putative motor regions based on connectivity with the precentral gyrus. Values in parentheses show the lower and upper bounds of the 95% confidence intervals of chance overlap based on a permutation test.

	Left Hemisphere			**Right Hemisphere**		
Structural / **Functional**	Caudate Convergence Zone	Putamen Convergence Zone	Putamen Motor	Caudate Convergence Zone	Putamen Convergence Zone	Putamen Motor
Caudate	70.23%* (0.2559, 0.2757)	31.21%* (0.1413, 0.1591)	25.70%* (0.0990, 0.1150)	66.67%* (0.2734, 0.3580)	61.74%* (0.2173, 0.3009)	52.75%* (0.1022, 0.1719)
Putamen	42.42%* (0.2734, 0.2816)	27.36%* (0.1510, 0.1583)	21.37%* (0.1065, 0.1128)	31.57%* (0.2191, 0.2271)	31.29%* (0.1696, 0.1771)	16.44%* (0.0887, 0.0951)
Motor	33.80% (0.3609, 0.3768)	30.75% (0.3369, 0.3536)	39.56% (0.3827, 0.3988)	20.92% (0.2634, 0.2823)	26.49% (0.2833, 0.3015)	50.50%* (0.3883, 0.4042)

* = significant observed overlap above chance